Magneto-Elastic Coupling in $RbMnF_3$†

D. E. EASTMAN
IBM Watson Research Center, Yorktown Heights, New York
(Received 16 November 1966)

Magneto-elastic (ME) coupling effects in the simple cubic antiferromagnet $RbMnF_3$ have been studied by observing shifts in antiferromagnetic resonance (AFMR) frequency and changes in AFMR line shape with the application of axial stress. Antiferromagnetic resonance in a two-sublattice antiferromagnet with a general anisotropy and ME interaction is analyzed. Formulas for the evaluation of ME constants of a two-sublattice cubic antiferromagnet are presented. ME constants of $RbMnF_3$ have been determined as a function of temperature from measurements of AFMR in single-crystal specimens under applied stress. The spin-lattice strain coefficients in the spin Hamiltonian for S-state Mn^{2+} in $RbMnF_3$ have been determined from experimental ME constants and calculated magnetic dipolar ME constants. Large changes in the static and dynamic response of low-anisotropy $RbMnF_3$ can be effected by the application of stress; via ME coupling, applied stress can change both the form and magnitude of the total anisotropy. The measured AFMR linewidth of $RbMnF_3$ at low temperatures is shown to be due to inhomogeneous strain broadening. The intrinsic relaxation linewidth is estimated to be less than 5 Oe.

INTRODUCTION

IT is well known[1] that anisotropy plays a key role in both the static and dynamic response of an antiferromagnet. In low-anisotropy antiferromagnets such as $RbMnF_3$ (H_A is about 4 Oe at 4.2°K), applied and inhomogeneous stresses have an especially large effect, since they cause significant changes in the total anisotropy via moderate magneto-elastic (ME) coupling. In this work, ME coupling effects in $RbMnF_3$ are investigated by studying antiferromagnetic resonance (AFMR) in single-crystal specimens subjected to applied stress.[2]

AFMR in a two-sublattice antiferromagnet with arbitrary anisotropy and magneto-elastic (ME) coupling subjected to applied stress has been analyzed. Application is made to cubic $RbMnF_3$, and formulas are presented for evaluating ME coupling constants. The ME constants of $RbMnF_3$ have been determined in the temperature range 4.2 to 83.0°K by measuring AFMR versus applied stress. The present technique circumvents the difficult problem of controlling sublattice magnetizations, which is encountered using conventional strain-gauge techniques. Because of the multidomain nature of cubic antiferromagnets, it is extremely difficult to control the sublattice magnetization orientation throughout a specimen with an applied field.

Large stress-dependent changes in the AFMR resonance field, linewidth, and line shape have been observed in $RbMnF_3$. Stress-dependent ME effects are much more accentuated in antiferromagnets than in ferro- or ferrimagnets because of the coupling of exchange and anisotropy in AFMR: a stress-dependent change in the anisotropy field δH_A shifts the AFMR resonance field $\delta H_r \simeq (H_E/H_r)\delta H_A$, where H_E is the exchange field. In the case of a ferromagnet, H_r is shifted $\delta H_r \simeq \delta H_A$.

At low temperatures, the observed AFMR linewidth in $RbMnF_3$ is due to inhomogeneous strain broadening. This occurs because of the large stress effect on AFMR and because there is no net long-range magnetic dipolar narrowing mechanism present in antiferromagnets to couple different regions together so that they assume a common resonance frequency.[3] Thus, an inhomogeneous internal field will fully contribute to the observed linewidth. Large changes in the linewidth and line shape as a function of stress have been observed which are explained by the presence of an inhomogeneous stress. Further evidence is furnished by the result that the ratio $\Delta H/(dH_r/dp)$ of the linewidth ΔH and stress derivative of the resonance field, dH_r/dp, is strongly correlated for a number of different experiments. From the experimental data, an upper bound of 5 Oe can be placed on the intrinsic relaxation linewidth.

The measured ME constants and estimated intrinsic linewidth indicate that phonon-pumped magnon instabilities[4] will have very low phonon-power thresholds of the order of 30 mW/cm² in $RbMnF_3$. As shown by Morgenthaler,[4] a phonon-pumped magnon instability experiment can be used to determine the spin-wave relaxation linewidth ΔH_k.

Another interesting experiment which appears to be feasible using $RbMnF_3$ is the direct observation of standing antiferromagnetic spin-wave modes in a thin disk. According to Orbach and Pincus,[5] the spacings of the spin-wave resonances are given by

$$\Delta\omega/\gamma \simeq (\omega_{res}/\gamma)(H_E/2H_A)\pi^2(a/L)^2 m,$$

for $H_0=0$, where H_A is the anisotropy field, a the lattice constant, L the disk thickness, and m an integer. In

† Work supported in part by the U. S. Air Force Office of Scientific Research of the Office of Aerospace Research under Contract No. AF 49(638)-1379.

[1] S. Foner, in *Magnetism*, edited by G. T. Rado and H. Suhl (Academic Press Inc., New York, 1963), Vol. I., p. 384.

[2] A brief report of this work has been published by D. E. Eastman, R. J. Joenk, and D. T. Teaney, Phys. Rev. Letters **17**, 300 (1966).

[3] A. M. Clogston, J. Appl. Phys. **29**, 334 (1958). In a ferrimagnet, because of dipolar narrowing, an inhomogeneous internal field ΔH_i will result in a resonance linewidth $\Delta H \simeq \Delta H_i^2/4M_s$ for $\Delta H_i \ll 4M_s$, where M_s is the saturation magnetization.

[4] F. R. Morgenthaler, Phys. Rev. Letters **14**, 907 (1965).

[5] R. Orbach and P. Pincus, Phys. Rev. **113**, 1213 (1959).

general, it is difficult to resolve spin-wave resonances since mode spacings are comparable to or narrower than linewidths. In $RbMnF_3$, however, the application of [001] stress induces a uniaxial [001] anisotropy which can result in a small anisotropy field, namely, $H_A \simeq H_N$, the nuclear hyperfine field.

In Sec. I, an analysis of AFMR in a two-sublattice antiferromagnet having an arbitrary anisotropy and applied stress is presented; application is made to cubic $RbMnF_3$. Experimental results are discussed in Sec. II and the origin and temperature dependence of the ME coupling is discussed in Sec. III.

I. ANTIFERROMAGNETIC RESONANCE IN $RbMnF_3$ IN THE PRESENCE OF APPLIED STRESS

A. General Considerations

The dynamic response of a stressed two-sublattice antiferromagnet is calculated by first determining the equilibrium orientation of the coupled sublattices and equilibrium strains and then applying appropriate dynamic torque equations for the two sublattices. Both the static and dynamic responses are conveniently obtained using a Gibbs "free"-energy density,[6] which has the following form for cubic $RbMnF_3$:

$$\begin{aligned} G&=E_{\text{exchange}}+E_{\text{Zeeman}}+E_{\text{hyperfine}}+E_A{}^{\text{cubic}} \\ &\quad +E_A{}^{\text{ME}}+E_{\text{mech}} \\ &=\lambda\mathbf{M}_1\cdot\mathbf{M}_2-\mathbf{H}_0\cdot(\mathbf{M}_1+\mathbf{M}_2)-H_N(\hat{I}_1\cdot\mathbf{M}_1+\hat{I}_2\cdot\mathbf{M}_2) \\ &\quad +K_1[(\alpha_1^2\alpha_2^2+\text{c.p.})+(\beta_1^2\beta_2^2+\text{c.p.})] \\ &\quad +B_1[(\alpha_1^2+\beta_1^2)\eta_{11}+\text{c.p.}]+B_2[(\alpha_1\alpha_2+\beta_1\beta_2)\eta_{12}+\text{c.p.}] \\ &\quad +B_3[\alpha_1\beta_1\eta_{11}+\text{c.p.}]+B_4[(\alpha_1\beta_2+\alpha_2\beta_1)\eta_{12}+\text{c.p.}] \\ &\quad +\tfrac{1}{2}c_{11}(\eta_{11}^2+\text{c.p.})+c_{12}(\eta_{11}\eta_{22}+\text{c.p.}) \\ &\quad +\tfrac{1}{2}c_{44}(\eta_{12}^2+\text{c.p.}), \end{aligned} \tag{1.1}$$

where λ is the Weiss exchange-field coefficient (λ equals H_E/M_s with H_E the exchange field and M_s the sublattice magnetization), $\mathbf{H}_0$ is the applied field, $\mathbf{M}_1$ and $\mathbf{M}_2$ are the sublattice magnetizations with direction cosines α_i and $\beta_i (i=1, 2, 3)$, respectively; $\hat{\alpha}$ and $\hat{\beta}$ are unit vectors parallel to $\mathbf{M}_1$ and $\mathbf{M}_2$, H_N is the nuclear hyperfine field ($H_N=9.43/T$ Oe for Mn^{55} in $RbMnF_3$ [7]), $\hat{I}_1$ and $\hat{I}_2$ are unit vectors in the nuclear-spin directions, K_1 is the first-order cubic magnetocrystalline anisotropy constant, $B_1 \cdots B_4$ are magnetoelastic coupling constants; η_{ij} are the strain coefficients,

$$\eta_{ij}=(1-\tfrac{1}{2}\delta_{ij})\left(\frac{\partial u_i}{\partial x_j}+\frac{\partial u_j}{\partial x_i}\right),$$

with u_i being the displacement vector, c_{11}, c_{12}, and c_{44} are the elastic constants, and c.p. denotes cyclic permutation of the indices 1, 2, 3. Dipolar demagnetizing field effects are neglected in Eq. (1.1). Only single-ion crystalline anisotropy is explicitly included in Eq. (1.1) since it adequately describes $RbMnF_3$,[7] while both single-sublattice (B_1 and B_2) and coupled-sublattice (B_3 and B_4) magneto-elastic energy terms are included.[8] It will be shown in Sec. III that one-ion (crystal-field origin) and two-ion (magnetic-dipolar origin) sources of magneto-elastic coupling are comparable in $RbMnF_3$. It is assumed that $|\mathbf{M}_1|=|\mathbf{M}_2|=M_s(T)$, i.e., the parallel susceptibility is neglected.[9] This assumption is valid for most antiferromagnets at low temperatures and is valid for all temperatures for high field resonance in the spin-flopped state.

The equilibrium orientations of $\mathbf{M}_1$ and $\mathbf{M}_2$ and equilibrium strains at fixed field and homogeneous applied stress σ_{ij} are found by minimizing G and are given by the 12 coupled equations.

$$(\partial G/\partial \mathbf{M}_1)\times\mathbf{M}_1=0, \tag{1.2a}$$

$$(\partial G/\partial \mathbf{M}_2)\times\mathbf{M}_2=0, \tag{1.2b}$$

$$(\partial G/\partial \eta_{ij})=\sigma_{ij}, \tag{1.2c}$$

subject to the constraints $\mathbf{M}_1\cdot\mathbf{M}_1=\mathbf{M}_2\cdot\mathbf{M}_2=\mathbf{M}_s^2$. The strains appear linearly in Eq. (1.2c) and are easily obtained in terms of $\hat{\alpha}_0$, $\hat{\beta}_0$, and σ_{ij}, where $\hat{\alpha}_0$ and $\hat{\beta}_0$ are the equilibrium values of $\hat{\alpha}$ and $\hat{\beta}$. They contain magnetostriction and applied stress contributions. These strains are then substituted in Eqs. (1.2a) and (1.2b) and $\hat{\alpha}_0$ and $\hat{\beta}_0$ can be determined. In the present work magnetostrictive strains ($\sim 10^{-6}$) are neglected compared to the stress-induced strains ($\sim 10^{-4}$).[10]

The equations of motion at constant strain are

$$\frac{1}{\gamma}\frac{d\mathbf{M}_1}{dt}=\mathbf{M}_1\times\mathbf{H}_1{}^{\text{eff}}, \tag{1.3}$$

with

$$\begin{aligned} \mathbf{H}_1{}^{\text{eff}}&=-\partial G/\partial\mathbf{M}_1 \\ &=-\lambda\mathbf{M}_2+\mathbf{H}_0+H_N\hat{I}_1 \\ &\quad -\frac{1}{M_s}\left(\frac{\partial E_A{}^{\text{cub}}}{\partial\hat{\alpha}}+\frac{\partial E_A{}^{\text{ME}}}{\partial\hat{\alpha}}\right), \end{aligned} \tag{1.4}$$

and with a similar equation for $\mathbf{M}_2$. The equations for the two sublattices are linearized in the usual way and can be reduced to a 4×4 coupled set of equations by using $x'y'z'$ and $x''y''z''$ axes for $\hat{\alpha}$ and $\hat{\beta}$ as follows:

$$\hat{\alpha}'=\mathcal{R}\hat{\alpha}, \tag{1.5a}$$

$$\hat{\beta}''=\mathcal{Q}\hat{\beta}. \tag{1.5b}$$

[6] W. F. Brown, *Micromagnetics* (Interscience Publishers, Inc., New York, 1963), see Chaps. 3 and 4.

[7] D. T. Teaney and M. J. Freiser, Phys. Rev. Letters **9**, 212 (1962).

[8] There are in general two more terms in $E_A{}^{\text{ME}}$, $B_0(\hat{\alpha}\cdot\hat{\alpha}+\hat{\beta}\cdot\hat{\beta})\times\sum_{(i)}\eta_{ii}+B_0'\hat{\alpha}\cdot\hat{\beta}\sum_{(i)}\eta_{ii}$, which are volume magnetostriction terms; these are neglected in this paper.

[9] See Ref. 1, p. 392.

[10] Using the experimental ME constants of Sec. II, it is found that the magnetostriction contribution to K_1 is approximately 5%.

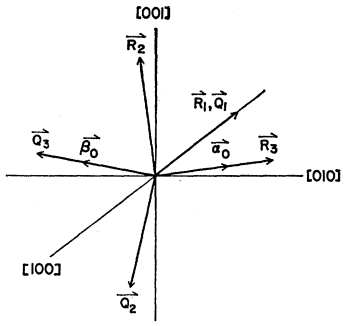

FIG. 1. The crystal coordinate system $x\ y\ z$ and transformed coordinate systems $x'y'z'$ $(\hat{R}_1,\hat{R}_2,\hat{R}_3)$ and $x''y''z''$ $(\hat{Q}_1,\hat{Q}_2,\hat{Q}_3)$ shown with $\hat{\alpha}_0$ and $\hat{\beta}_0$ in the yz plane.

Here $\mathcal{Q}$ is a 3×3 unitary matrix which transforms the column vector $\hat{\alpha}$ in the crystal coordinate system into $\hat{\alpha}'$ in the $x'y'z'$ system. The row vectors of $\mathcal{R}$, which are denoted as $\hat{R}_1$, $\hat{R}_2$, and $\hat{R}_3$, are unit vectors in the $\hat{\beta}_0\times\hat{\alpha}_0$, $\hat{\alpha}_0\times(\hat{\beta}_0\times\hat{\alpha}_0)$, and $\hat{\alpha}_0$ directions.[11] Similarly, the row vectors $\hat{Q}_1$, $\hat{Q}_2$, and $\hat{Q}_3$ of $\mathcal{Q}$ are unit vectors in the $\hat{\beta}_0\times\hat{\alpha}_0$, $\hat{\beta}_0\times(\hat{\beta}_0\times\hat{\alpha}_0)$, and $\hat{\beta}_0$ directions. The various unit vectors $\hat{R}_1$, etc. are shown in Fig. 1; $\hat{\alpha}_0$ and $\hat{\beta}_0$ are parallel to $\hat{z}'$ and $\hat{z}''$, respectively. The linearized equations of motion for $\delta\boldsymbol{\alpha}'=\hat{\alpha}'-\hat{\alpha}_0'$ and $\delta\boldsymbol{\beta}''=\hat{\beta}''-\hat{\beta}_0''$ are then

$$\frac{1}{\gamma}\begin{vmatrix}\delta\dot{\alpha}_1'\\ \delta\dot{\alpha}_2'\\ \delta\beta_1''\\ \delta\beta_2''\end{vmatrix}=\begin{vmatrix} a & b & e & f\\ c & -a & g & h\\ -h & f & a' & b'\\ g & -e & c' & -a'\end{vmatrix}\begin{vmatrix}\delta\alpha_1'\\ \delta\alpha_2'\\ \delta\beta_1''\\ \delta\beta_2''\end{vmatrix},\tag{1.6}$$

with

$$\begin{aligned}
a&=M_s^{-1}\hat{R}_2\cdot\nabla_\alpha\nabla_\alpha G^0\cdot\hat{R}_1,\\
b&=M_s^{-1}(-\hat{R}_3\cdot\nabla_\alpha G^0+\hat{R}_2\cdot\nabla_\alpha\nabla_\alpha G^0\cdot\hat{R}_2),\\
c&=M_s^{-1}(-\hat{R}_3\cdot\nabla_\alpha G^0-\hat{R}_1\cdot\nabla_\alpha\nabla_\alpha G^0\cdot\hat{R}_1),\\
e&=M_s^{-1}\hat{R}_2\cdot\nabla_\alpha\nabla_\beta G^0\cdot\hat{Q}_1,\\
f&=M_s^{-1}\hat{R}_2\cdot\nabla_\alpha\nabla_\beta G^0\cdot\hat{Q}_2,\\
g&=-M_s^{-1}\hat{R}_1\cdot\nabla_\alpha\nabla_\beta G^0\cdot\hat{Q}_1,\\
h&=-M_s^{-1}\hat{R}_1\cdot\nabla_\alpha\nabla_\beta G^0\cdot\hat{Q}_2,
\end{aligned}$$

and a', b', and c' are obtained from a, b, and c by replacing $\hat{R}_{(i)}$ by $\hat{Q}_{(i)}$, ∇_α by ∇_β, and ∇_β by ∇_α. In Eq. (1.6), $\nabla_\alpha\equiv\partial/\partial\hat{\alpha}$, $(\nabla_\alpha\nabla_\alpha G)_{ij}=\partial^2G/\partial\alpha_i\alpha_j$, and $\nabla_\alpha\nabla_\alpha G^0$ denotes the equilibrium value. The relation $\mathbf{V}_1\cdot\nabla_\alpha\nabla_\beta G^0\cdot\mathbf{V}_2=\mathbf{V}_2\cdot\nabla_\beta\nabla_\alpha G^0\cdot\mathbf{V}_1$, where $\mathbf{V}_1$ and $\mathbf{V}_2$ are arbitrary vectors, has been used in deriving Eq. (1.6). It has been assumed that the nuclear spins can not follow the rapidly varying electron spins, with the result that the hyperfine interaction contributes a uniaxial field H_N along the equilibrium spin direction. This assumption must be reexamined if the AFMR frequency is near the nuclear-magnetic-resonance (NMR) frequency or if low-frequency field modulation is present.

A significant simplification in Eq. (1.6) occurs if sublattice canting (angle $\lesssim H_0/2H_E$) is neglected in the evaluation of crystalline anisotropy and magnetoelastic terms in the coefficients $a\cdots h$. This is an excellent approximation for $RbMnF_3$, since H_E is $\sim$890 kOe, $H_0\lesssim10$ kOe, and the total anisotropy H_A is ~4 Oe. In this approximation, terms of order $H_A(H_0/H_E)$ are neglected compared to H_E, H_0^2/H_E, and H_A. The resulting coefficients $a\cdots h$ in Eq. (1.6) then become

$$\begin{aligned}
a&=M_s^{-1}(\hat{R}_2\cdot\nabla_\alpha\nabla_\alpha E_A{}^0\cdot\hat{R}_1),\\
b&=-H_E\hat{\alpha}_0\cdot\hat{\beta}_0+H_N+\hat{\alpha}_0\cdot\mathbf{H}_0+M_s^{-1}(-\hat{\alpha}_0\cdot\nabla_\alpha E_A{}^0\\
&\qquad+\hat{R}_2\cdot\nabla_\alpha\nabla_\alpha E_A{}^0\cdot\hat{R}_2),\\
c&=+H_E\hat{\alpha}_0\cdot\hat{\beta}_0-H_N-\hat{\alpha}_0\cdot\mathbf{H}_0+M_s^{-1}(\hat{\alpha}_0\cdot\nabla_\alpha E_A{}^0\\
&\qquad-\hat{R}_1\cdot\nabla_\alpha\nabla_\alpha E_A{}^0\cdot\hat{R}_1),\\
e&=M_s^{-1}\hat{R}_2\cdot\nabla_\alpha\nabla_\beta E_A{}^0\cdot\hat{R}_1,\\
f&=H_E\hat{\alpha}_0\cdot\hat{\beta}_0-M_s^{-1}\hat{R}_2\cdot\nabla_\alpha\nabla_\beta E_A{}^0\cdot\hat{R}_2,\\
g&=-H_E-M_s^{-1}\hat{R}_1\cdot\nabla_\alpha\nabla_\beta E_A{}^0\cdot\hat{R}_1,\\
h&=M_s^{-1}\hat{R}_1\cdot\nabla_\alpha\nabla_\beta E_A{}^0\cdot\hat{R}_2,\\
a'&=-a,\\
b'&=b+(\hat{\beta}_0-\hat{\alpha}_0)\cdot\mathbf{H}_0,\\
c'&=c-(\hat{\beta}_0-\hat{\alpha}_0)\cdot\mathbf{H}_0,
\end{aligned}\tag{1.7}$$

where $E_A{}^0$ equals $E_A{}^{\rm cub}$ plus $E_A{}^{\rm ME}$ evaluated at equilibrium (with $\hat{\beta}_0=-\hat{\alpha}_0$) and $\hat{R}_2$ is a unit vector along $\mathbf{H}_0$.[12] The relations $\hat{\beta}_0\cdot\nabla_\beta E_A{}^0=\hat{\alpha}_0\cdot\nabla_\alpha E_A{}^0$ and $\nabla_\beta\nabla_\beta E_A{}^0=\nabla_\alpha\nabla_\alpha E_A{}^0$ have been used. These result from the symmetry $E_A(\alpha,\beta)=E_A(\beta,\alpha)$ and the condition that only terms having even powers in magnetization components are permitted in E_A. The eigenfrequencies of Eq. (1.6) with $a\cdots h$ as given in Eq. (1.7) are

$$\left(\frac{\omega}{\gamma}\right)^2=H_E(h_1+h_2)+(\hat{\alpha}_0\cdot\mathbf{H}_0)^2\pm\{H_E{}^2[(h_1-h_2)^2+4h_3{}^2]+H_E(h_1+h_2)[(\hat{\alpha}_0-\hat{\beta}_0)\cdot\mathbf{H}_0]^2\}^{1/2},\tag{1.8}$$

with

$$\begin{aligned}
h_1&=H_N+\tfrac{1}{2}(\hat{\alpha}_0+\hat{\beta}_0)\cdot\mathbf{H}_0+M_s^{-1}[-\hat{\alpha}_0\cdot\nabla_\alpha E_A{}^0+\hat{R}_2\\
&\qquad\cdot(\nabla_\alpha\nabla_\alpha E_A{}^0-\nabla_\alpha\nabla_\beta E_A{}^0)\cdot\hat{R}_2],\\
h_2&=H_N+\tfrac{1}{2}(\hat{\alpha}_0+\hat{\beta}_0)\cdot(\mathbf{H}_0-2\hat{\alpha}_0H_E)+M_s^{-1}[-\hat{\alpha}_0\\
&\qquad\cdot\nabla_\alpha E_A{}^0+\hat{R}_1\cdot(\nabla_\alpha\nabla_\alpha E_A{}^0-\nabla_\alpha\nabla_\beta E_A{}^0)\cdot\hat{R}_1],\\
h_3&=M_s^{-1}\hat{R}_2\cdot[\nabla_\alpha\nabla_\alpha E_A{}^0-\tfrac{1}{2}(\nabla_\alpha\nabla_\beta E_A{}^0+\nabla_\beta\nabla_\alpha E_A{}^0)]\cdot\hat{R}_1.
\end{aligned}\tag{1.9}$$

Equation (1.8) is valid for a two-sublattice antiferromagnetic with an arbitrary form of small (i.e., $H_A\ll H_E$) anisotropy for field strengths $H_0\lesssim\frac{1}{10}H_E$ at low temperatures. It is valid for all temperatures in the spin-flopped state. For high-field spin-flopped resonance

[11] If $\hat{\beta}_0\times\hat{\alpha}_0=0$, any convenient direction perpendicular to $\hat{\alpha}_0$ can be selected for $\hat{R}_1$.

[12] M. J. Freiser, R. J. Joenk, P. E. Seiden, and D. T. Teaney, in *Conference on Magnetism* (The Institute of Physics and The Physical Society, London, 1965), p. 432, have derived a set of resonance equations similar to Eqs. (1.6) and (1.7) for zero stress; however, there is a sign error (they have $a'=+a$ in the present notation) which can have important consequences for AFMR at fields near and below the "flop" field$\simeq(2H_EH_A)^{1/2}$.

$(H_0^2 \gg H_E H_A)$, Eq. (1.8) becomes simply

$$(\omega_1/\gamma)^2 = 2H_E h_1, \tag{1.10a}$$

$$(\omega_2/\gamma)^2 = 2H_E h_2, \tag{1.10b}$$

where h_1 is field-dependent and h_2 is field-independent.

B. High-Field Resonance

In the high-field spin-flopped limit $(H_0^2 \gg H_E H_A)$, the AFMR eigenfrequencies are relatively simple. From Eqs. (1.8)–(1.10), one obtains the field-dependent and field-independent frequencies

$$(\omega_1/\gamma)^2 = H_0^2 + 2H_E(H_N + H_A{}^{(1)}), \tag{1.11a}$$

$$(\omega_2/\gamma)^2 = 2H_E(H_N + H_A{}^{(2)}), \tag{1.11b}$$

with

$$H_A{}^{(1)} = M_s{}^{-1}[-\hat{\alpha}_0 \cdot \nabla_\alpha E_A{}^0 + \hat{R}_2 \cdot (\nabla_\alpha \nabla_\alpha E_A{}^0 - \nabla_\alpha \nabla_\beta E_A{}^0) \cdot \hat{R}_2], \tag{1.12a}$$

$$H_A{}^{(2)} = M_s{}^{-1}[-\hat{\alpha}_0 \cdot \nabla_\alpha E_A{}^0 + \hat{R}_1 \cdot (\nabla_\alpha \nabla_\alpha E_A{}^0 - \nabla_\alpha \nabla_\beta E_A{}^0) \cdot \hat{R}_1], \tag{1.12b}$$

where $E_A (= E_A{}^{\text{cub}} + E_A{}^{\text{ME}})$ is the total effective anisotropy at fixed strain and $H_A{}^{(1)}$ and $H_A{}^{(2)}$ are the effective resonance anisotropy fields. In Eq. (1.12), $\hat{R}_2 = \hat{l}$, a unit vector along $\mathbf{H}_0$, and $\hat{R}_1 = \hat{l} \times \hat{\alpha}_0$.

For $RbMnF_3$, using the Gibbs function of Eq. (1.1), $\nabla_\alpha \nabla_\beta E_A{}^0$ is proportional to $\nabla_\alpha \nabla_\alpha E_A{}^0$. Therefore, only two linear combinations of the magneto-elastic constants $B_1 \cdots B_4$, namely,

$$b_1 = B_1 - \tfrac{1}{2}B_3, \tag{1.13a}$$

$$b_2 = B_2 - B_4, \tag{1.13b}$$

are involved in the resonance frequencies.[13] The AFMR frequencies can then be described using a single-sublattice form of magneto-elastic coupling,

$$E_A = b_1[(\alpha_1^2 + \beta_1^2)\eta_{11} + \text{c.p.}] + b_2[(\alpha_1\alpha_2 + \beta_1\beta_2)\eta_{12} + \text{c.p.}], \tag{1.14}$$

with b_1 and b_2 given by Eq. (1.13).

The effective anisotropy fields $H_A{}^{(1)}$ and $H_A{}^{(2)}$ contain cubic-anisotropy and magneto-elastic terms. The cubic-anisotropy terms, which can be obtained from Eq. (1.12), have been evaluated previously[7,14]:

$$H_A{}^{(1)\text{cub}} = \tfrac{3}{2}H_A f_1(\alpha_0), \tag{1.15a}$$

$$H_A{}^{(2)\text{cub}} = \tfrac{3}{2}H_A f_2(\alpha_0), \tag{1.15b}$$

with

$$f_1 = 3\textstyle\sum_{(i)} l_i^2 \alpha_{0i}^2 - \sum_{(i)} \alpha_{0i}^4, \tag{1.16a}$$

$$f_2 = 3 - 3\textstyle\sum_{(i)} l_i^2 \alpha_{0i}^2 - 4\sum_{(i)} \alpha_{0i}^4, \tag{1.16b}$$

$$H_A = -4K_1/(3M_s).$$

The magneto-elastic-field terms in $H_A{}^{(1)}$ and $H_A{}^{(2)}$ are determined using Eqs. (1.12) and (1.14). Expressed in terms of the applied stress σ_{ij}, they are

$$H_A{}^{(1)\text{ME}} = -2b_1 s_{11} M_s{}^{-1}[\sigma_{11}(\alpha_{01}^2 - l_1^2) + \text{c.p.}] - 2b_1 s_{12} M_s{}^{-1}[(\sigma_{22} + \sigma_{33})(\alpha_{01}^2 - l_1^2) + \text{c.p.}] - 2b_2 s_{44} M_s{}^{-1}[\sigma_{12}(\alpha_{01}\alpha_{02} - l_1 l_2) + \text{c.p.}], \tag{1.17}$$

with $H_A{}^{(2)\text{ME}}$ given by $H_A{}^{(1)\text{ME}}$ with l_i replaced by $(\hat{l} \times \hat{\alpha}_0)_i \equiv n_i$. In Eq. (1.17), s_{ij} are the elastic compliance coefficients.

The special cases of [001] and [1$\bar{1}$0] applied stress with $\mathbf{H}_0$ perpendicular to the applied stress are relatively simple and permit evaluation of b_1 and b_2. These cases have been considered experimentally.

For [001] compressive stress, $\sigma_{33} = -p$, with $p > 0$, and one has

$$E_A{}^{\text{ME}} = K\alpha_{03}^2, \tag{1.18a}$$

$$H_A{}^{(1)\text{ME}} = H_1(\alpha_{03}^2 - l_3^2), \tag{1.18b}$$

with

$$H_1 = -\frac{2K}{M_s} = \frac{2b_1 p}{M_s(c_{11} - c_{12})}. \tag{1.18c}$$

Here H_1 represents the stress-induced anisotropy field. The stress-dependent spin direction $\hat{\alpha}_0$ and resonance frequencies for [001] stress are summarized in Table I.[15] The normalized stress $x = K/K_1 = 2H_1/3H_A$ can be positive or negative according to the sign of b_1. It is observed that the magnetization direction $\hat{\alpha}_0$ and the AFMR frequencies, especially the field-independent mode, are strongly dependent on the applied stress. The AFMR is uniaxial in nature for $x > 1$; this has been observed in $RbMnF_3$. Various features of the resonances in Table I will be discussed in Sec. II.

For [1$\bar{1}$0] uniaxial stress, $\sigma_{11} = \sigma_{22} = -\sigma_{12} = -p/2$, and one has

$$E_A{}^{\text{ME}} = \tfrac{1}{2}M_s H_1 \alpha_{03}^2 + \tfrac{1}{2}M_s H_2 \alpha_{01}\alpha_{02}, \tag{1.19a}$$

$$H_A{}^{(1)\text{ME}} = -\tfrac{1}{2}H_1(\alpha_{03}^2 - l_3^2) - H_2(\alpha_{01}\alpha_{02} - l_1 l_2), \tag{1.19b}$$

with

$$H_2 = b_2 p/(M_s c_{44}). \tag{1.19c}$$

There is considerable algebraic complexity for $\mathbf{H}_0$ in an arbitrary direction in the [1$\bar{1}$0] plane. Therefore, two cases, namely, with $\mathbf{H}_0$ along [110] and [001], are considered. Experimentally, these cases are convenient since they are insensitive to slight misorientations. Results are summarized in Table I. The normalized stress is $x' = 2(H_1 + H_2)/3H_A$.

The magneto-elastic constants b_1 and b_2 [more precisely, the quantities $(H_E b_1)/[M_s(c_{11} - c_{12})]$ and $(H_E b_2)/(M_s c_{44})$] are most conveniently determined from the field-dependent resonances by measuring H_0 versus pressure at fixed frequency. For this purpose the pres-

[13] This is also true for low-field resonance; see Eq. (1.9).

[14] M. J. Freiser, P. E. Seiden, and D. T. Teaney, Phys. Rev. Letters 10, 293 (1963).

[15] In Table I, the formulas for $\hat{\alpha}_0$ neglect spin canting. The spins are canted toward $\mathbf{H}_0$ from the given directions by an angle ψ with $\sin\psi = H_0/2H_E$.

TABLE I. Summary of AFMR for [001] and [1̄10] applied stress.

Stress region[a]	Magnetization direction $\hat{\alpha}_0$	Resonance frequencies
I. [001] stress, $\mathbf{H}_0$ along $(l_1,l_2,0)$.		
(a) $-\frac{1}{4}(3+\cos4\phi)<x<1$	$\left(\mp l_2\frac{1-x}{2(1-l_1^2l_2^2)},\ \pm l_1\frac{1-x}{2(1-l_1^2l_2^2)},\ 1-\frac{(1-x)}{2(1-l_1^2l_2^2)}\right)$	$\left(\frac{\omega_1}{\gamma}\right)^2=H_0^2+2H_EH_N+3H_EH_A(1-x)\frac{-4\cos4\phi}{7+\cos4\phi}$ $\left(\frac{\omega_2}{\gamma}\right)^2=2H_EH_N+3H_EH_A\left[\frac{6+2\cos4\phi}{7+\cos4\phi}+x\left(\frac{2-2\cos4\phi}{7+\cos4\phi}\right)+x^2\left(\frac{-8}{7+\cos4\phi}\right)\right]$
(b) $x>1$	$(-0,0,1)$	$\left(\frac{\omega_1}{\gamma}\right)^2=H_0^2+2H_EH_N+3H_EH_A(x-1)$ $\left(\frac{\omega_2}{\gamma}\right)^2=2H_EH_N+3H_EH_A(x-1)$
(c) $x<-\frac{1}{4}(3+\cos4\phi)$	$(-l_2,l_1,0)$	$\left(\frac{\omega_1}{\gamma}\right)^2=H_0^2+2H_EH_N-3H_EH_A\cos4\phi$ $\left(\frac{\omega_2}{\gamma}\right)^2=2H_EH_N+3H_EH_A[-x-\frac{1}{4}(3+\cos4\phi)]$
II. [1$\bar{1}$0] stress, H_0 along $[1/\sqrt{2},\ 1/\sqrt{2},\ 0]$.		
(a) $-2<x'<1$	$\left(\left(\frac{2+x'}{6}\right)^{1/2},\ -\left(\frac{2+x'}{6}\right)^{1/2},\ \left(\frac{1-x'}{3}\right)^{1/2}\right)$	$\left(\frac{\omega_1}{\gamma}\right)^2=H_0^2+2H_EH_N+2H_EH_A+\frac{2}{3}H_E(H_1+4H_2)$ $\left(\frac{\omega_2}{\gamma}\right)^2=2H_EH_N+H_EH_A[2-x'-(x')^2]$
(b) $x'>1$	$(1/\sqrt{2},\ -1\sqrt{2},\ 0)$	$\left(\frac{\omega_1}{\gamma}\right)^2=H_0^2+2H_EH_N+3H_EH_A+2H_EH_2$ $\left(\frac{\omega_2}{\gamma}\right)^2=2H_EH_N+\frac{3}{2}H_EH_A(x'-1)$
(c) $x'<-2$	$(0,0,1)$	$\left(\frac{\omega_1}{\gamma}\right)^2=H_0^2+2H_EH_N-3H_EH_A-H_E(H_1-H_2)$ $\left(\frac{\omega_2}{\gamma}\right)^2=2H_EH_N+\frac{3}{2}H_EH_A(-x'-2)$
III. [1$\bar{1}$0] stress, H_0 along [001].		
(a) $H_2>0$	$(-1/\sqrt{2},\ 1/\sqrt{2},\ 0)$	$\left(\frac{\omega_1}{\gamma}\right)^2=H_0^2+2H_EH_N-\frac{3}{2}H_EH_A+H_E(H_1+H_2)$ $\left(\frac{\omega_2}{\gamma}\right)^2=2H_EH_N+3H_EH_A+2H_EH_2$
(b) $H_2<0$	$(-1/\sqrt{2},\ 1/\sqrt{2},\ 0)$	$\left(\frac{\omega_1}{\gamma}\right)^2=H_0^2+2H_EH_N-\frac{3}{2}H_EH_A+H_E(H_1-H_2)$ $\left(\frac{\omega_2}{\gamma}\right)^2=2H_EH_N+3H_EH_A-2H_EH_2$

[a] $x=-\frac{2}{3}\frac{H_1}{H_A}$, $x'=-\frac{2}{3}\frac{H_1+H_2}{H_A}$, $H_1=\frac{2b_1p}{(c_{11}-c_{12})M_s}$, $H_2=\frac{b_2p}{c_{44}M_s}$, $l_1=\cos\phi$, $l_2=\sin\phi$.

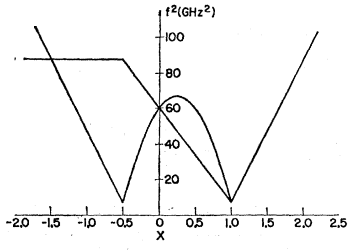

FIG. 2. Zero-field AFMR versus stress in $RbMnF_3$ at $T=20°K$. The values $H_E=880$ kOe, $H_A=3.8$ Oe, and $H_N=0.47$ Oe have been used. The normalized stress is calculated to be $x=2.3\times10^{-3}\,p$.

sure derivatives

$$\frac{dH_1}{dp}=\frac{2b_1}{M_s(c_{11}-c_{12})} \quad \text{and} \quad \frac{dH_2}{dp}=\frac{b_2}{M_s c_{44}}$$

are evaluated in terms of dH_0/dp in Table II.

C. Zero-Field Resonance

At zero field, the resonance frequency is proportional to the geometric mean of the exchange and anisotropy fields. For $RbMnF_3$ applied uniaxial stress can alter the anisotropy from cubic to uniaxial in nature, thereby causing very large AFMR frequency shifts. As an example, zero-field resonance under [001] uniaxial stress is considered. Then all four possible equilibrium spin directions are equivalent and a single-domain situation exists experimentally. The equilibrium spin direction $\hat{\alpha}_0$ and resonance frequencies are determined using Eqs. (1.8) and (1.9) and are given by the results Ia, Ib, and Ic in Table I with H_0 set equal to zero.

The resonance frequencies, which exhibit very large shifts, are shown in Fig. 2. Measured magneto-elastic constants have been used. At stresses above $x=1$ (i.e., ~400 bars), the anisotropy is uniaxial and a single magnetic domain exists. Experimentally, stresses of $x\simeq2.0$ at 4.2°K have been applied during high-field resonance experiments. Zero-field resonance has not been measured.

TABLE II. Determination of b_1 and b_2.[a]

(Ia)	$\frac{4\cos4\phi}{7+\cos4\phi}\frac{dH_1}{dp}=-\frac{H_0}{H_E}\frac{dH_0}{dp}$
(Ib)	$\frac{dH_1}{dp}=-\frac{H_0}{H_E}\frac{dH_0}{dp}$
(Ic)	$0=\frac{dH_0}{dp}$
(IIa)	$\frac{1}{3}\left(\frac{dH_1}{dp}+4\frac{dH_2}{dp}\right)=-\frac{H_0}{H_E}\frac{dH_0}{dp}$
(IIb)	$\frac{dH_2}{dp}=-\frac{H_0}{H_E}\frac{dH_0}{dp}$
(IIc)	$\frac{1}{2}\left(\frac{dH_1}{dp}-\frac{dH_2}{dp}\right)=\frac{H_0}{H_E}\frac{dH_0}{dp}$
(IIIa)	$\frac{1}{2}\left(\frac{dH_1}{dp}+\frac{dH_2}{dp}\right)=-\frac{H_0}{H_E}\frac{dH_0}{dp}$
(IIIb)	$\frac{1}{2}\left(\frac{dH_1}{dp}-\frac{dH_2}{dp}\right)=-\frac{H_0}{H_E}\frac{dH_0}{dp}$

[a] From measurement of H_0 versus stress at fixed frequency. Experiments Ia, etc., are defined in Table I.

II. EXPERIMENTAL RESULTS

AFMR in the spin-flopped state in $RbMnF_3$ has been measured as a function of uniaxial stress and temperature at a frequency of 23 GHz. These measurements have verified various features of the calculated AFMR modes described in Sec. I, have determined the magneto-elastic constants b_1 and b_2 as a function of temperature, and have demonstrated the important effect of inhomogeneous strains on the AFMR linewidth.

A. Spin-Flopped Resonance with [001] and [1$\bar{1}$0] Stress

Spin-flopped AFMR with $\mathbf{H}_0$ perpendicular to an applied [001] stress has been studied since it is relatively simple to interpret and permits the determination of the magneto-elastic constant b_1 [see Eq. (1.14)]. The observed resonance field versus stress relations for $\mathbf{H}_0$ in the [100] and [110] directions are shown in Fig. 3. Figure 3 indicates that the induced anisotropy field H_1 [see Eq. (1.18c)] is positive. Thus, as the compressive stress is increased from zero, the spins rotate toward the [001] axis in the plane perpendicular to $\mathbf{H}_0$ until, at the turning point stress $x=1$ ($p=420$ bars), they become parallel to the [001] stress direction (neglecting canting). For x greater than unity, the induced uniaxial anisotropy is greater than the intrinsic cubic anisotropy (the spins remain parallel to [001] and the resonance field is independent of the orientation of $\mathbf{H}_0$ in the [001]

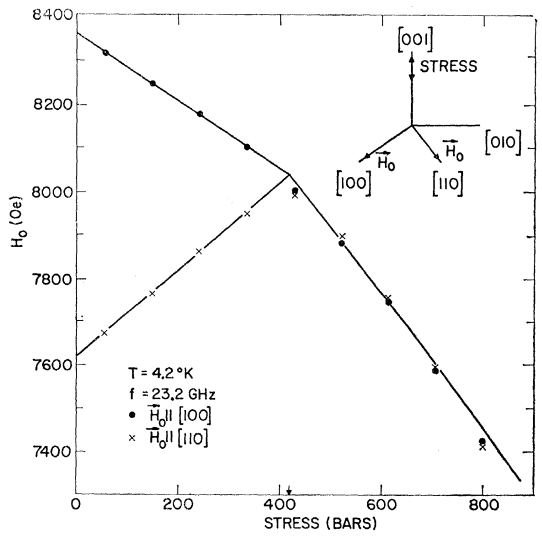

FIG. 3. Resonance field H_0 versus applied [001] stress. $H_E=8.9\times10^5$ Oe, $H_A=3.8$ Oe, $H_N=2.22$ Oe, $b_1=1.5\times10^6$ erg/cm³.

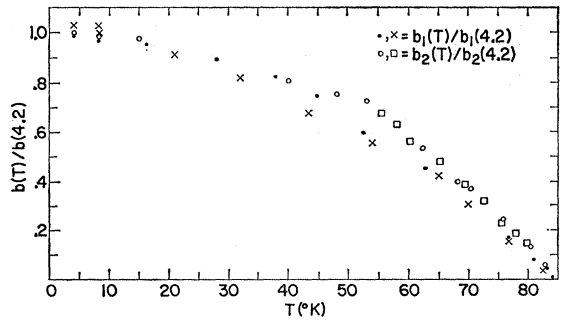

FIG. 4. Temperature dependence of b_1 and b_2; T_N=83.0°K.

plane), as shown in Fig. 3. The solid lines show the predicted results (see Ia, Ib, Ic in Table I) using the experimentally determined $H_1(p)$. The normalized ratios of the slopes of the three straight-line segments in Fig. 3 have the calculated values $(-1):(4/3):(-2)$, and the experimental agreement is excellent.

The magneto-elastic constant b_1 {actually $H_1=2b_1p/[(c_{11}-c_{12})M_s]$} has been measured from 4.2°K to the Néel temperature T_N=83.0°K by measuring H_0 versus stress with $\mathbf{H}_0$ along [100], as shown in Fig. 3. The temperature dependence of $b_1(T)$ is proportional to the measured quantity $H_EH_1 \propto \lambda M_s(T)\cdot[b_1(T)/M_s(T)]$ assuming the elastic constants and Weiss field coefficient λ are independent of temperature. In Fig. 4, the normalized magneto-elastic constant $b_1(T)/b_1(4.2)$ is plotted as a function of temperature for two different crystals. At 4.2°K, b_1 has been determined from the measurement of H_EH_1 as

$$b_1=(1.5\pm0.15)\times10^6 \text{ erg/cm}^3,$$

using M_s=304 G (theoretical), measured value[8] H_E=890 kOe, and measured elastic constants which are discussed in Sec. IID.

Spin-flopped AFMR with [1$\bar{1}$0] stress permits the determination of b_1 and b_2. Typical data with $\mathbf{H}_0$ along [110] and [001] are shown in Fig. 5. These directions are convenient since they are insensitive to small misalignments of field and are simple to interpret. In Fig. 5, at the turning-point stress $x'=1(p=390$ bars), the slope of H_0 versus x' changes with $\mathbf{H}_0$ along [110], while no change is observed with $\mathbf{H}_0$ along [001]. These measurements are in accord with the calculated results in Table I.

Both the magnitude and sign of b_1 and b_2 can be determined using the three slopes shown in Fig. 5 and the appropriate formulas listed in Table II. Using Fig. 5 and the formulas in Table II, one finds that $x'\geq0$ for compressive stress. Thus, b_2 can be directly and most accurately determined from high-stress data ($x'>1$) with $\mathbf{H}_0$ along [110] (see IIb in Tables I and II).[16] In this manner, b_2 has been determined at 4.2°K as

$$b_2=(0.16\pm0.02)\times10^6 \text{ erg/cm}^3$$

using the above-mentioned H_E, M_s, and elastic constants. The temperature dependence of b_2, measured in the above manner using two different crystals, is shown in Fig. 4.

B. Linewidth Studies

The AFMR linewidth and line shape are strongly affected by inhomogeneous stress. At low temperatures the observed linewidth is due to inhomogeneous broadening of the AFMR and is not an intrinsic relaxation linewidth. These conclusions are based on a number of AFMR stress effects which have been observed.

First, with (1$\bar{1}$0) stress and $\mathbf{H}_0$ along [110] (see Fig. 5), the linewidth has been observed to decrease abruptly from $2\Delta H\simeq175$ Oe to $2\Delta H\simeq75$ Oe as the stress is increased through the turning-point value $x'=1$. This corresponds to the observed change in stress sensitivity $|dH_0/dp|$ and indicates that the observed linewidth is due to inhomogeneous stress. Also, a sharp edge in the line shape develops at a field strength corresponding to the turning-point stress, thereby indicating an intrinsic linewidth much narrower than the observed linewidth.

Further evidence is given by Fig. 6, which shows the absorption x'' versus field with [001] stress as a parameter and with $\mathbf{H}_0$ along [110]. A plot of the resonance field H_0 versus stress for this case is given in Fig. 3. It is seen from Fig. 3 (and Table I) that no resonance field greater than the resonance field at the turning point, $H_0=[(\omega/\gamma)^2-2H_EH_N]^{1/2}=8040$ Oe, should be observed. As shown in Fig. 6, a sharp edge in the line

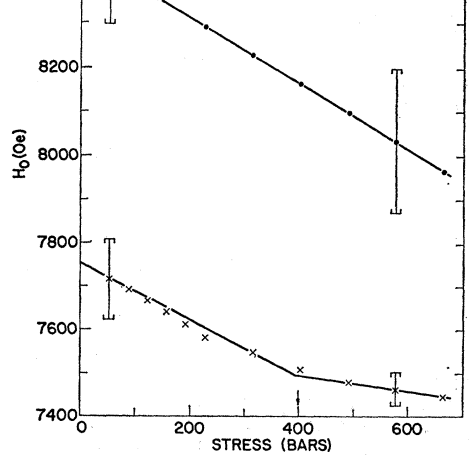

FIG. 5. Resonance field H_0 versus applied [1$\bar{1}$0] stress. H_E =8.9×10^5 Oe, H_N=2.0 Oe. Best fit is H_A=3.7 Oe, $b_1=(1.3\pm.15)\times10^6$ erg/cm^3, $b_2=(0.17\pm0.02)\times10^6$ erg/cm^3.

[16] These data are used to determine b_2 while b_1 is determined from [001] stress data. It is difficult to obtain low-stress ($x'<1$) data with $\mathbf{H}_0$ along [110] at temperatures above approximately 30°K because the cubic anisotropy becomes small.

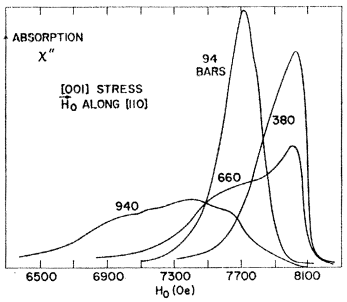

FIG. 6. Absorption χ'' versus applied field with [001] stress as a parameter. F=23.2 GHz.

shape occurs at this field, with very little absorption at higher fields. The line shape is symmetrical for stresses well below and well above the turning-point stress, and near the turning point the observed line shape can be described by folding a symmetrical line shape about the maximum resonance field. These results strongly suggest inhomogeneous strain broadening.

A strong correlation in $\Delta H/|dH_0/dp|$ has been observed for all measurements at low temperatures. At higher temperatures, the observed linewidth becomes less sensitive to stress and less correlation in $\Delta H/|dH_0/dp|$ was observed. At the Néel temperature the linewidth was unaffected by stress.

Further evidence of inhomogeneous broadening is furnished by the observation that line shapes are generally Gaussian at low temperatures and are Lorentzian at high temperatures near the Néel temperature. At low temperatures, an estimate of the inhomogeneous stress half-width Δp, assuming $\Delta p \simeq \Delta H/|dH_0/dp|$, is $\Delta p \simeq 150$ bars.[17,18]

A bound on the intrinsic linewidth ΔH_0 can be estimated based on the sharpness of the observed edges in the absorption line shape at the turning-point stress. The estimated bound is $\Delta H_0 \lesssim 5$ Oe. Heeger and Pincus[19] and Heeger[20] have measured the AFMR linewidth as $\Delta H \simeq 40$ Oe in $KMnF_3$; it should have an inhomogeneous stress broadening comparable to $RbMnF_3$. They have also measured a critical rf field ($h_c=0.2$ Oe) for spin-wave instability at 1.8°K. The critical rf field h_c is related to the uniform precession relaxation linewidth ΔH_0 and spin-wave relaxation linewidth ΔH_k by[19]

$$h_c = 4\Delta H_0[\Delta H_k/2H_E H_{A1}]^{1/2},$$

with $2H_E H_{A1}$ equal to 3200 Oe. Heeger and Pincus obtained the anomalously small spin-wave linewidth $\Delta H_k = 5\times10^{-3}$ Oe upon assuming that the relaxation linewidth ΔH_0 is equal to the observed linewidth $\Delta H = 40$ Oe. However, it is known from the present studies that the uniform mode is inhomogeneously broadened. An estimate of ΔH_k can be made, which represents an upper bound, by assuming that different regions of the crystal are uncorrelated. Then, assuming that $\Delta H_0 \simeq \Delta H_k$, as is observed in ferrimagnets such as yttrium iron garnet, one obtains

$$\Delta H_0 \simeq \Delta H_k \simeq 2 \text{ Oe}$$

for $KMnF_3$ from the data of Heeger.[20] This result is in accord with the above estimated bound on ΔH_0 for $RbMnF_3$.

C. Experimental Methods

The measurement technique consists of measuring microwave AFMR in single-crystal specimens which are subjected to uniaxial stress.[21] Rectangular parallelopiped specimens with polished parallel faces and linear dimensions of 45–65 mils were used.[22] The stress was applied to the specimens using two 2-mm silica quartz rods with parallel endfaces which extended out through the microwave cavity. The stress was generated using a set of calibrated weights and a push rod extending down to the cavity. A metal jacket enclosing the cavity (with a metal bellows arrangement for the push rod) contained helium gas and coupled the cavity and specimen to a liquid-helium (or liquid-nitrogen) temperature bath. The cavity resonance, at 23 GHz, was independent of stress as the force load was supported by the metal vacuum jacket. Direct dc detection and a very low Q cavity ($Q \simeq 15$) were used.

A platinum resistance sensor and dc heater with a feedback system were used to control temperature to ±0.2°K in the range of 12 to 85°K. Temperatures below 12°K were controlled manually and were measured to ±1°K using a Au-Co thermocouple and/or platinum resistance sensor.

D. Determination of Elastic Moduli

The elastic moduli of cubic $RbMnF_3$ were determined at room temperature using the pulsed ultrasonic system

TABLE III. Measurement of ultrasonic velocity.

Propagation direction	Wave polarization	Measured velocity V (cm/sec)	Calculated velocity
[100][a]	longitudinal, $\mathbf{u}\parallel$[100]	4.93×10^5	$(c_{11}/\rho_0)^{1/2}$
[100][a]	shear, $\mathbf{u}\perp$[100]	2.64×10^5	$(c_{44}/\rho_0)^{1/2}$
[110][b]	shear, $\mathbf{u}\parallel$[010]	2.64×10^5	$(c_{44}/\rho_0)^{1/2}$
[110][b]	shear, $\mathbf{u}\parallel$[110]	2.88×10^5	$((c_{11}-c_{12})/2\rho_0)^{1/2}$
[110][b]	longitudinal, $\mathbf{u}\parallel$[110]	4.91×10^5	$((c_{11}+c_{12}+2c_{44})/2\rho_0)^{1/2}$

[a] $l=7.122\pm0.005$ mm.
[b] $l=6.335\pm0.005$ mm. $\mathbf{u}$=elastic polarization, ρ_0=mass density.

[17] As a rough order-of-magnitude comparison, the inhomogeneous stress measured by Feher (Ref. 18) for Mn^{2+} in MgO is ~100 bar. The inhomogeneous strain corresponding to 150 bar for $RbMnF_3$ is $\Delta\eta \simeq 1.5\times10^{-4}$.
[18] E. Feher, Phys. Rev. **136**, A145 (1964).
[19] A. J. Heeger and P. Pincus, Phys. Rev. Letters **10**, 53 (1963).
[20] A. J. Heeger, Phys. Rev. **131**, 608 (1963).
[21] A. B. Smith and R. V. Jones, J. Appl. Phys. **34**, 1283 (1963).
[22] Included were specimens prepared from crystals grown by Semielements, Inc.

of Toxen and Tansal.[23] Shear and longitudinal waves were generated at 10 and 30 MHz using $\frac{1}{8}$-in.-diam *ac*-cut and *x*-cut quartz transducers with a 10-MHz fundamental frequency. Nonaq stopcock grease was used to bond the transducers to the specimen. A pair of parallel polished [100] faces spaced 7.122 mm and a pair of [110] faces spaced 6.335 mm were prepared on the same single-crystal specimen.

Measured ultrasonic velocities for the five acoustic modes propagating in the [100] and [110] crystal directions are summarized in Table III. The velocities were determined according to

$$V=2l/2t,$$

where l is the acoustic path length and $2t$ is the observed two-way acoustic delay time between adjacent ultrasonic echoes. Using the theoretical density $\rho_0=4.30$ g/cm^3, the elastic moduli were determined from the data in Table III in units of 10^{11} dyn/cm^2 as

$$c_{11}=10.45,\quad c_{12}=3.32,\quad c_{44}=3.00.$$

Estimated accuracies are ± 2, 7, and 1%, respectively.

III. ORIGIN AND TEMPERATURE DEPENDENCE OF b_1 AND b_2

The magnetoelastic constants b_1 and b_2 have the values listed in Table IV at 4.2°K. The magnetic-dipolar interaction is dependent on strain through the interionic distance and contributes to the ME coupling. This contribution has been calculated assuming localized moments. This assumption should be quite good for *S*-state Mn^{2+} ions. The magnetic-dipolar ME interaction can be written in the form given by $E_A{}^{ME}$ in Eq. (1.1). The calculated contributions to $B_1 \cdots B_4$ at 0°K are

$$\Delta B_1=-\tfrac{1}{4}(g\beta S/2a_0{}^3)^2\Sigma_1,$$
$$\Delta B_2=\tfrac{1}{6}(g\beta S/2a_0{}^3)^2\Sigma_1,$$
$$\Delta B_3=\tfrac{1}{4}(g\beta S/2a_0{}^3)^2\Sigma_2,$$
$$\Delta B_4=-\tfrac{1}{12}(g\beta S/2a_0{}^3)^2\Sigma_2,$$

where g is the Landé factor, β the Bohr magneton, S the spin quantum number ($S=\frac{5}{2}$), and a_0 the lattice constant (4.24 Å). The dimensionless dipole sums Σ_1 and Σ_2 are

$$\Sigma_1=7.69,\quad \Sigma_2=127.4,$$

for a simple-cubic antiferromagnetic lattice.

TABLE IV. Origin of b_1 and b_2.

	Origin	
(a) Measured[a]	(b) Dipolar	(c) Difference (a)−(b)
$b_1=1.4\times10^6$ erg/cm^3	$\Delta b_1=-1.65\times10^6$	$\delta b_1=+3.05\times10^6$
$b_2=0.17\times10^6$	$\Delta b_2=+1.10\times10^6$	$\delta b_2=-0.93\times10^6$

[a] $T=4.2$°K.

[23] A. M. Toxen and S. Tansal, Phys. Rev. **137**, A211 (1965). A commercial Arenberg pulsed oscillator, preamplifier, and rf amplifier, and a sampling oscilloscope and *x-y* recorder are used.

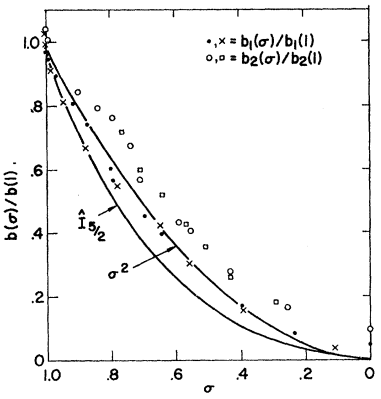

FIG. 7. Normalized magnetoelastic constants b_1 and b_2 versus normalized sublattice magnetization σ.

The calculated dipolar contributions to b_1 and b_2,

$$\Delta b_1=\Delta B_1-\tfrac{1}{2}\Delta B_3,$$
$$\Delta b_2=\Delta B_2-\Delta B_4,$$

are summarized in Table IV.

The difference between measured ME constants and calculated dipolar contributions,

$$\delta b_1=b_1-\Delta b_1,$$
$$\delta b_2=b_2-\Delta b_2,$$

are reasonably assumed to be of single-ion crystal-field origin.[24] The constants δb_1 and δb_2 can be related to a strain-dependent noncubic spin Hamiltonian H_{nc} as defined by Feher,[18]

$$H_{nc}=\mathbf{S}\cdot\mathbf{D}\cdot\mathbf{S}$$
$$=G_{11}\{[\eta_{11}-\tfrac{1}{2}(\eta_{22}+\eta_{33})]S_1{}^2+\text{c.p.}\}$$
$$+G_{44}[\eta_{12}(S_1S_2+S_2S_1)+\text{c.p.}],$$

where η_{ij} are the strain components and S_i is the ith Cartesian component of the spin operator. The strain coefficients G_{11} and G_{44} are related to δb_1 and δb_2 at $T=0$°K according to

$$G_{11}=4a_0{}^3\delta b_1/[3S(S-\tfrac{1}{2})],$$
$$G_{44}=a_0{}^3\delta b_2/[S(S-\tfrac{1}{2})],$$

for $S\geq 1$. G_{11} and G_{44} for Mn^{2+} in $RbMnF_3$ are then determined using δb_1 and δb_2 in Table IV as

$$G_{11}=0.31\text{ cm}^{-1},\quad G_{44},=-0.073\text{ cm}^{-1}.$$

For comparison, G_{11} and G_{44} have been determined for Mn^{2+} in MgO by Feher[18] as

$$G_{11}=1.49\text{ cm}^{-1},\quad G_{44}=-0.315\text{ cm}^{-1}.$$

[24] Anisotropic interactions such as anisotropic exchange contain the factor $(g-2)^2$ and will be very small as the g factor of the *S*-state Mn^{2+} is very nearly 2 [$g=2.0014$ for Mn^{2+} in MgO, see W. Low, Phys. Rev. **105**, 793 (1957)]. See J. Kanamori, in *Magnetism*, edited by G. T. Rodo and H. Suhl (Academic Press Inc., New York, 1963), Vol. I, Secs. (III, 4) and (IV).

In both cases Mn^{2+} is in an octahedral site, with a 4.24-Å F^-–F^- distance in $RbMnF_3$ and a 4.20-Å O^{2-}–O^{2-} distance in MgO. It is interesting to observe that the ratio G_{11}/G_{44} is -4.6 for Mn^{2+} in $RbMnF_3$ and -4.7 for Mn^{2+} in MgO.

The dependence of b_1 and b_2 on the normalized sublattice magnetization σ is shown in Fig. 7. It has been assumed that σ varies with temperature according to a Brillouin function for spin $\frac{5}{2}$. The temperature dependence predicted by the single-ion theory of Callen and Callen[25,26] is shown by the solid line. According to Refs. 25 and 26, if b_1 and b_2 are of a single-ion nature, they should vary as

$$b(\sigma)=\frac{I_{5/2}(L^{-1}(\sigma))}{I_{1/2}(L^{-1}(\sigma))}\equiv\hat{I}_{5/2}(\sigma),$$

where $I_{l+1/2}$ is the hyperbolic Bessel function and L^{-1} is the inverse Langevin function. The above relation results from a classical spin average in the molecular field approximation.[25,26] $\hat{I}_{5/2}$ is nearly equal to σ^3 over most of the range of σ.

According to Callen and Callen,[27] magnetic dipolar ME coupling should vary as σ^2 except at very low temperatures. It is seen from Fig. 7 that the experimental b_1 and b_2 are not described by either the $I_{5/2}$ or σ^2 curves. These data support the above conclusions that both single-ion and magnetic dipolar ME coupling are comparable in magnitude.

[25] E. R. Callen and H. B. Callen, Phys. Rev. **129**, 578 (1963).
[26] E. R. Callen, A. E. Clark, B. DeSavage, and W. Coleman, Phys. Rev. **130**, 1735 (1963).

ACKNOWLEDGMENTS

It is a pleasure to acknowledge D. T. Teaney and R. J. Joenk for many valuable discussions; D. T. Teaney also supplied the $RbMnF_3$ crystals and R. J. Joenk calculated the magnetic dipolar ME constants. A. M. Toxen was of considerable help in furnishing equipment and assistance for the ultrasonic measurement of elastic constants.

[27] E. Callen and H. B. Callen, Phys. Rev. **139**, 455 (1965).

PHYSICAL REVIEW VOLUME 156, NUMBER 2 10 APRIL 1967

Ferrimagnetic and Antiferromagnetic Structures of Cr_5S_6†

B. VAN LAAR
Reactor Centrum Nederland, Petten, The Netherlands
(Received 14 October 1966)

An investigation of the magnetic and the nuclear structures of Cr_5S_6 at four different temperatures has been carried out by means of neutron diffraction. It has been found that in the nuclear structure, deviations from the idealized structure as given by Jellinek are small at all temperatures. The magnetic structure of the antiferromagnetic phase is an antiferromagnetic screw-type spiral with its propagation vector along the c axis. The spin structure in the ferrimagnetic state is collinear and strongly related to the antiferromagnetic structure. Experimental results show that the transition from the antiferromagnetic to the ferrimagnetic state is coupled to the occurrence of a noncollinear component of the moment on the $4f$ sites.

INTRODUCTION

THE crystal structure of Cr_5S_6 has been deduced by Jellinek.[1] It can be considered as a NiAs-type structure in which one of each six Cr atoms has been removed, leading to completely ordered vacancies. The structure as given by Jellinek is

space group: $P\bar{3}1c$ (D_{3d}^2);
2 Cr in 2(a): $0,0,\frac{1}{4}$;
2 Cr in 2(c): $\frac{1}{3},\frac{2}{3},\frac{1}{4}$;
2 Cr in 2(b): $0,0,0$; $0,0,\frac{1}{2}$;
4 Cr in 4(f): $\frac{1}{3},\frac{2}{3},z$; $\frac{1}{3},\frac{2}{3},\frac{1}{2}-z$ with $z=0$;
12S in 12(i): x,y,z; $\bar{y},x-y,z$; $y-x,\bar{x},z$; $y,x,\frac{1}{2}+z$;
$x-y,y,\frac{1}{2}+z$; $\bar{x},y-x,\frac{1}{2}+z$,
with $x=\frac{1}{3}$, $y=0$, $z=\frac{3}{8}$.

At room temperature, the lengths of the unit-cell edges are $a=5.982$ Å and $c=11.509$ Å, and the cell volume is six times that of the NiAs-type subcell.

The magnetic properties of Cr_5S_6 have been the subject of many studies.[2–8] The compound is antiferromagnetic below 168°K, in the sense that there is no net magnetic moment, ferrimagnetic between 168 and 303°K, and paramagnetic above 303°K. Kamigaichi[4]

† Work sponsored jointly by Reactor Centrum Nederland, The Netherlands and Institutt for Atomenergi, Norway.
[1] F. Jellinek, Acta Cryst. **10**, 620 (1957).
[2] H. Haraldsen and A. Neuber, Z. Anorg. Allgem. Chem. **234**, 337 (1937).
[3] M. Yuzuri, T. Hirone, H. Watanabe, S. Nagasaki, and S. Maeda, J. Phys. Soc. Japan **12**, 385 (1957).
[4] T. Kamigaichi, J. Sci. Hiroshima Univ., Ser. A **24**, 371 (1960).
[5] M. Yuzuri, Y. Kang, and Y. Goto, J. Phys. Soc. Japan **17**, Suppl. B1, 253 (1962).
[6] K. Dwight, R. W. Germann, N. Menyuk, and A. Wold, J. Appl. Phys. Suppl. **33**, 1341 (1962).
[7] M. Yuzuri and Y. Nakamura, J. Phys. Soc. Japan **19**, 1350 (1964).
[8] C. F. van Bruggen and F. Jellinek, Colloque International sur les dérivées semi métalliques du Centre National de la Recherche Scientifique, Orsay, 1965 (to be published).